Fabrication of chirped and multi–period waveguide embedded Bragg gratings in lithium niobate

S. Kroesen,* J. Imbrock, and C.Denz

Institute of Applied Physics and Center for Nonlinear Science, University of Muenster, Corrensstr. 2-4, 48149 Muenster, Germany

ABSTRACT

We demonstrate monolithic fabrication of tunable, waveguide embedded Bragg gratings (WBG) in lithium niobate by direct femtosecond laser writing. Complex refractive index modulation profiles such as chirped and multi periodic gratings are inscribed into the core volume of a circular, two-dimensional waveguide structure. The hybrid type-I/II design that consists of a type-II waveguide and a type-I multiscan grating exhibits low loss symmetric guiding of ordinary and extraordinary polarized modes and narrowband reflections in the c-band of optical communications. High bandwidth spectral tunability of more than a peak half width and nearly preserved electro–optic coefficients of $r_{13} = 7.67\,\mathrm{pm\,V^{-1}}$ and $r_{33} = 24.7\,\mathrm{pm\,V^{-1}}$ are realized.

Keywords: Laser material processing, Lithium niobate, Integrated optics devices, Waveguides, Bragg reflectors, Optoelectronics, Three-dimensional fabrication

1. INTRODUCTION

Optical waveguides and integrated optical devices are fundamental components of optical communications and signal processing. In addition to common lithographic techniques, direct femtosecond laser writing is nowadays recognized as a versatile tool to inscribe arbitrary three-dimensional refractive index landscapes into various materials including glasses, crystals and ceramics.[1–3] Particularly with respect to direct integration of functional optical devices it is indispensable to inscribe waveguide structures, couplers, and gratings into nonlinear optical materials to exploit their inherent reconfigurability.[4] However, in contrast to most isotropic materials where a positive refractive index modification can be achieved inside the focal volume of the writing beam, the intrinsic anisotropy of crystalline materials complicate direct write approaches and new complex designs and writing schemes are required.[5,6]

In this contribution we present a hybrid design that consists of a circular type-II waveguide and an embedded type-I Bragg grating.[6] The structure supports both, ordinary and extraordinary polarized modes, which is mandatory to access features based on the largest electro–optic coefficient r_{33} for extraordinary polarization. Second order Bragg gratings with specific refractive index modulation profiles e. g. uniform, multi–period and linearly chirped are inscribed into the waveguide core using a multiscan technique with high transverse resolution. Finally, narrow spaced integrated electrodes are realized using femtosecond laser material ablation. We demonstrate that the waveguide embedded Bragg gratings (WBG) exhibit low loss symmetric guiding and narrowband reflections in the c-band of optical communications. Moreover, we show high bandwidth spectral tuning of more than a peak half width and nearly preserved electro–optic coefficients.

2. DIRECT FEMTOSECOND LASER WRITING: WAVEGUIDES AND OPTICAL DEVICES IN CRYSTALLINE MATERIALS

The most essential property of direct laser writing approaches with respect to integrated optics and fabrication of guided wave devices is the induced refractive index change. The sign, strength and spatial extent of the modification determines possible inscription geometries and the application potential. Besides material–specific properties, the induced refractive index change depends on inscription parameters such as pulse duration, pulse energy, repetition rate, translation velocity and numerical aperture of the employed microscope objective.[3]

*s.kroesen@uni-muenster.de

Advanced Fabrication Technologies for Micro/Nano Optics and Photonics VIII, edited by Georg von Freymann, Winston V. Schoenfeld, Raymond C. Rumpf, Proc. of SPIE Vol. 9374, 937404 · © 2015 SPIE
CCC code: 0277-786X/15/$18 · doi: 10.1117/12.2079871

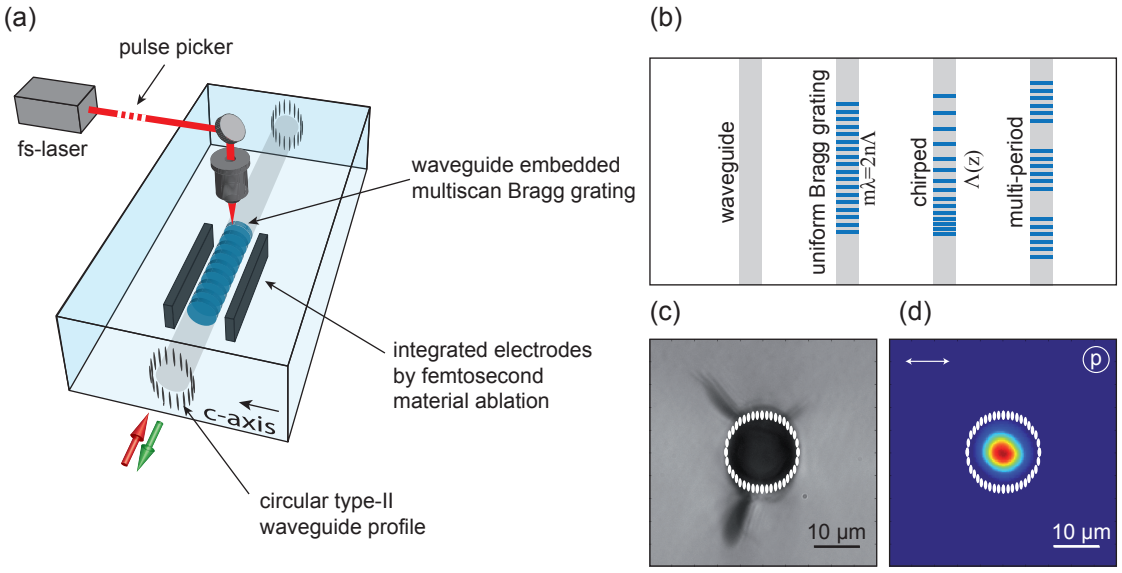

Figure 1. (a) Schematic of the waveguide embedded Bragg grating (WBG) design that consists of a circular type-I waveguide, a multiscan Bragg grating and integrated electrodes. (b) Different grating types such as uniform, chirped and multi–period Bragg gratings. (c) Coupling facet of a *closed circular* type-II waveguide and (d) corresponding near field mode profile for extraordinary input polarization at 1.505 µm, where the position of individual filaments is indicated by the white elongated spots.

The physical origin of the refractive index modulation in lithium niobate is nontrivial and has been discussed by various authors.[7–10] We follow the most common classification of type–I and type–II material modifications. In the first case, which is associated with very low laser fluences, an increased refractive index is observed in the irradiated regions. The latter case obtained for higher laser fluences is associated with the creation of an amorphous filament and subsequent reduction of the refractive index inside the focal volume. The guiding properties of type-II structures are primary determined by the two–dimensional stress field distribution imposed to the crystal lattice and thus can be tailored by the writing geometry.[11] In general, both types of refractive index modulation are strongly anisotropic and the nonlinear coefficients of the processed material are not necessarily preserved, which is a bottleneck for efficient frequency conversion and electro–optic devices.[10,12]

2.1 Experimental configuration for WBG inscription

A schematic of the experimental setup and WBG design is shown in Fig. 1(a). The system is based on an Ytterbium–doped Potassium Gadolinium Tungstate (Yb:KGW) femtosecond laser system with up to 2 mJ pulse energy at $\lambda = 1028$ nm central wavelength and a three–dimensional translation stage with nanometer precision. The repetition rate of the laser system is adjustable over a large range reaching from single shot operation to 600 kHz, which enables fast inscription sequences with translation velocities of the order of several millimeters per second. The laser power that is used for either strong type-II waveguides lines or significantly weaker type-I multiscan sequences, is precisely adjusted by an interchangeable set of neutral density filers in combination with a half wave plate and a polarizing beam splitter. We use commercially available x–cut lithium niobate wafers with a thickness of 500 µm, which are cut into 10×10 mm^2 samples and subsequently polished to optical quality. All presented structures are fabricated at a depth of 100 µm below the surface using a microscope objective with a numerical aperture of NA $= 0.8$.

2.2 Two–dimensional waveguide geometry

Type-II waveguides with permanent, high contrast refractive index profiles can be created for a large range of parameters. Typically, double–line structures are inscribed with pulse energies from 200 nJ to 750 nJ and

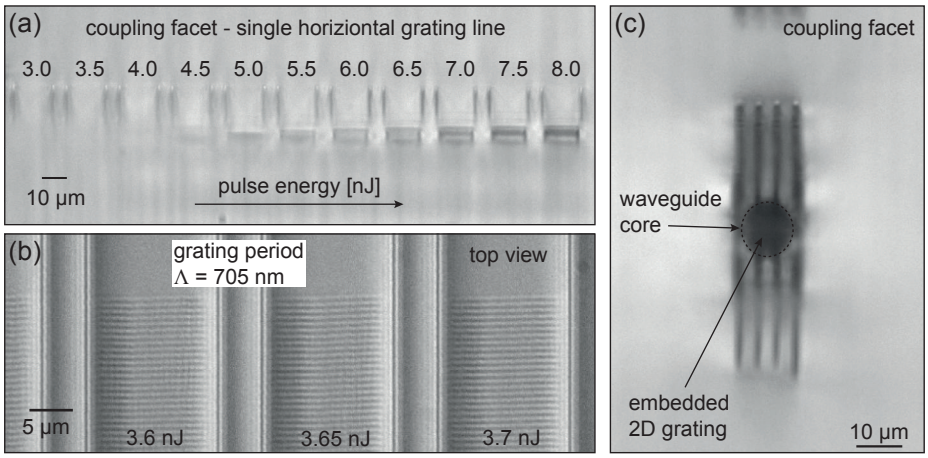

Figure 2. Optical microscope images of the multiscan Bragg grating. (a) Front facet of a single horizontal grating line as a function of the pulse energy; the confining lines are inscribed with 105 nJ for clear imaging of the type-I/type-II filamentation process. (b) Top–view of a selected energy area; the period of 705 nm is clearly visible. (c) Coupling facet of a rectangular waveguide with an embedded Bragg grating centered inside the waveguide core.

$3\,\mathrm{mm\,s^{-1}}$ to $8\,\mathrm{mm\,s^{-1}}$ (100 kHz repetition rate). These basic structures exhibit strong polarization dependence and asymmetric guiding properties. Particularly extraordinary polarized light is often weakly confined making these structures inadequate for many nonlinear devices. Most recently, two–dimensional circular waveguide designs referred to as depressed cladding–, or type–III waveguides have been proposed that overcome these limitations and provide nearly balanced, low loss guidance along both input polarizations.[5,13–15]

A more detailed analysis on two–dimensional waveguides and different writing geometies can be found in our previous work.[6] Here we primary focus on embedded Bragg gratings, thus we just briefly review the parameters used for waveguide inscription. A microscope image of a typical *closed–circular* waveguide and the associated extraordinary polarized mode is shown in Figs. 1(c) and 1(d). The positions of the individual lines that are inscribed with a pulse energy of 65 nJ, are indicated by the elongated white spots. We found that for the given refractive index contrast a diameter or clear aperture of 12 µm to 15 µm is well suited to enable single mode transmission. A mode circularity of 99.5 % and −4.94 dB insertion loss for extraordinary polarization is obtained for a 10 mm long waveguide. In summary, the presented closed–circular waveguide exhibits pure single–mode propagation for both, ordinary and extraordinary polarized light with an average propagation loss of $(1.1 - 1.6)\,\mathrm{dB\,cm^{-1}}$ of ordinary–, and $(3.0 - 3.8)\,\mathrm{dB\,cm^{-1}}$ for extraordinary polarization, making them an ideal base component for nonlinear integrated optical devices.

2.3 Fabrication of embedded multiscan Bragg gratings

Second–order Bragg gratings with a period of $\Lambda = 700\,\mathrm{nm}$ to $\Lambda = 708\,\mathrm{nm}$ are realized using a multiscan technique.[16] In contrast to direct point–by–point integration of strong type-II gratings,[12] where the periodic modulation is achieved indirectly by the outer waveguide lines, the entire core volume of the waveguide is successively scanned and modified. Technically the method is based on the so called position synchronous output (PSO) provided by the fast electronics of the translation stage. A TTL signal is generated after a defined travel distance, which is used to unlock the pulse–picker (PP) of the laser system. The major advantage with respect to point–by–point schemes is the possibility to apply arbitrary modulation functions. Multi–period gratings, phase–shifted, superstructures or chirped Bragg gratings can directly be inscribed without any demand for specific lithographic masks. Moreover, this method is independent of deviations of the translation velocity and therefore less sensitive to perturbations.

A typical type-I Bragg grating sequence is inscribed with very low pulse energies of several nanojoules and reduced translation velocity of $0.3\,\mathrm{mm\,s^{-1}}$ to improve positioning stability (10 kHz). A transverse multiscan

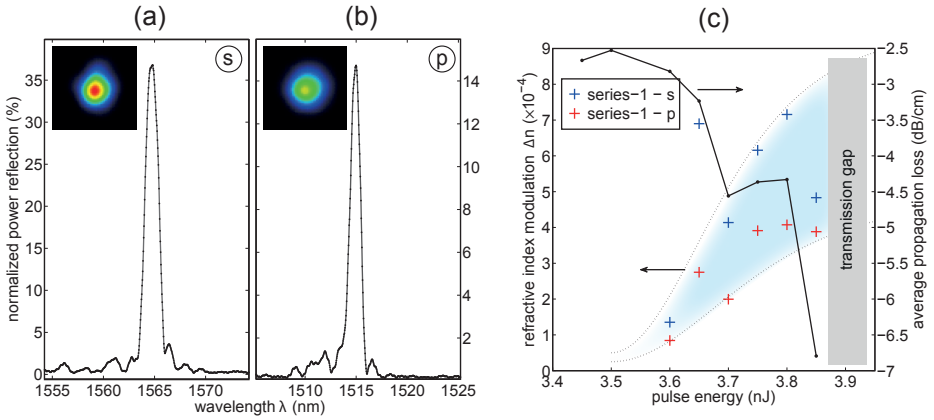

Figure 3. (a) Experimental reflection spectra for ordinary and (b) extraordinary input polarization and corresponding mode profiles (inset). (c) Refractive index modulation (i. e. coupling strength) and average propagation loss versus pulse energy that is used for the grating sequence. It can be clearly seen that the operation window of the type-I/type-II filamentation process is very narrow and follows a tanh–characteristic centered around 3.7 nJ.

resolution of 300 nm in horizontal, and 700 nm in vertical direction is used, respectively. Fig. 2(a) shows the polished front facet of different multiscan Bragg gratings, where the upper and lower waveguide lines are omitted for clear imaging. A complete series with increasing pulse energies reaching from 3 nJ to 8 nJ is inscribed to visually determine the threshold pulse energy of a starting type-II filamentation process. Within our experimental conditions (pulse duration and focusing conditions) the type-I/II threshold is around 4 nJ. Hence, the ideal operation window for the multiscan sequence is approximately 3.4 nJ to 3.85 nJ. The unprocessed material and the smooth periodic modulation of the second order grating are clearly visible c. f. Fig. 2(b). It is important to correctly center the Bragg grating inside the waveguide core as shown in Fig. 2(c) to ensure a high spatial overlap of the guided mode and the grating (depicted for a so called *quad–waveguide*). It should be mentioned that pulse energies as high as 8 nJ completely destroy the waveguide core and potentially lead to cracked regions of the lithium niobate substrate. Careful adjustment of the employed pulse energy and good long term stability are mandatory to realize high quality WBG with reproducible coupling strength.

2.4 Integrated electrodes by femtosecond laser material ablation

As a final step, integrated electrodes are fabricated by femtosecond material ablation.[17,18] We use a 20 × microscope objective with a numerical aperture of NA = 0.55 and 12 µJ pulse energy. The volume of the u–grooves is scanned with a transverse resolution of 15 µm, 2 cm s^{-1} and 100 kHz. The total depth of the electrodes is matched to the fabrication depth of the WBGs to ensure a uniform electric field distribution along the Bragg grating. Subsequently, the grooves are filled with conductive silver, insulated to avoid voltage breakdown and connected to a high voltage amplifier. An electrode distance of d = 115 µm down to d = 64 µm with parallel surfaces is realized without any derogation to the waveguiding properties.

2.5 Waveguide Bragg grating characterization

Characterization of the inscribed WBGs is performed using a tunable laser source in a typical fiber–coupling arrangement. The cleaved fiber is coupled to the substrate after passing through a circulator, which is employed to analyze the reflection properties of the Bragg gratings. The power reference is obtained by coupling the fiber to a high reflective dielectric mirror. The near–field mode profile at the exit facet is imaged onto an InGaAs camera. To investigate linear ordinary-, and extraordinary polarization, a fiber squeezer is used in combination with a polarizing beam splitter in front of the camera. Insertion loss measurements are also conducted for all presented waveguide configurations employing a calibrated detector.

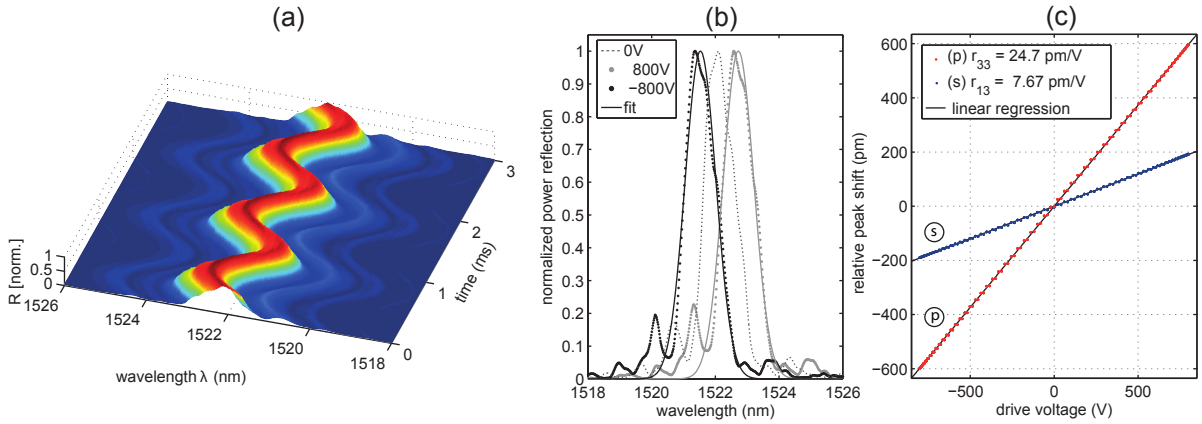

Figure 4. (a) Electro–optical tuning of a 1 mm long WBG structure with an electrode spacing of 115 µm and a modulation frequency of 1 kHz. (b) Reflection spectra at the maximum drive voltage of ±800 V for extraordinary polarized light. (c) Relative shift of the central reflection maxima versus drive voltage for both, ordinary– and extraordinary polarized light. Electro–optical tuning of a peak half width and nearly preserved nonlinear coefficients of $r_{13} = 7.67\,\mathrm{pm\,V^{-1}}$ and $r_{33} = 24.7\,\mathrm{pm\,V^{-1}}$ are obtained with a perfectly linear response.

3. CHARACTERIZATION OF WAVEGUIDE EMBEDDED BRAGG GRATINGS

The presented waveguide embedded Bragg gratings are fabricated in a bottom–up approach. First of all the bottom lines of the circular waveguide are inscribed at 100 kHz and $8\,\mathrm{mm\,s^{-1}}$ followed by the multiscan sequence at reduced velocity and the top waveguide lines at high velocity again. Since the core volume of the waveguide is scanned approximately 300 times, the total inscription duration of the presented structures is of the order of 40 min, which requires high long term stability of the writing system.

3.1 Reflection spectra of WBGs and induced grating strength

To analyze coupling strength and spectral properties of embedded Bragg gratings, a series of second–order WBGs with increasing grating strength is inscribed. The individual Bragg gratings are embedded into a 10 mm long closed–circular waveguide with an inset of 1 mm with respect to the front facet as indicated in Fig. 1(a). Pulse energies from 3.6 nJ to 4.05 nJ are selected to cover the ideal type-I operation window that reaches from no detectable refractive index modulation to a starting type-II filamentation process. Figure 3(a) and Fig. 3(b) show the power reflection spectra of one particular WBG inscribed with a pulse energy of 3.8 nJ. The associated mode profile is given in the inset. A power reflection of approximately 37 % for (a) s–polarized, and 15 % for (b) p–polarized light is achieved with narrow reflection bandwidth. The wavelength offset of the central Bragg reflection maxima ($\lambda_o - \lambda_e = 49.8\,\mathrm{nm}$) corresponds to the birefringence of lithium niobate. Effective refractive indices of $n_o = 2.204$ and $n_e = 2.134$ are calculated for an addressed period of $\Lambda = 708\,\mathrm{nm}$.

We performed numerical calculations to estimate the effective refractive index modulation for the entire series of WBGs as shown in Fig. 3(c). The induced refractive index modulation follows a tanh–characteristic centered around 3.7 nJ within our experimental configuration. The energy threshold of the type–II filamentation process is around 3.9 nJ for the high resolution multiscan approach. As a consequence, the power transmission decreases for an increasing grating strength limiting the applicable refractive index modulation to values of $\Delta n_{o,e} < 1 \times 10^{-3}$, which is in good agreement with the typical refractive index change obtained for type–I modifications.[11]

4. ELECTRO–OPTICAL TUNING

Nonlinear electro–optic tuning is performed for a 1 mm long WBG structure with an electrode spacing of 115 µm as shown Fig. 4(a). The Bragg grating inscribed with a pulse energy of 3.7 nJ exhibits a reflectivity of 25 % and narrow $1/e^2$ width of $\Delta\lambda = 1.14\,\mathrm{nm}$. A sinusoidal drive signal with a modulation frequency of 1 kHz and an amplitude of ±800 V is applied. The power reflection spectra at the maximum applied voltage and the

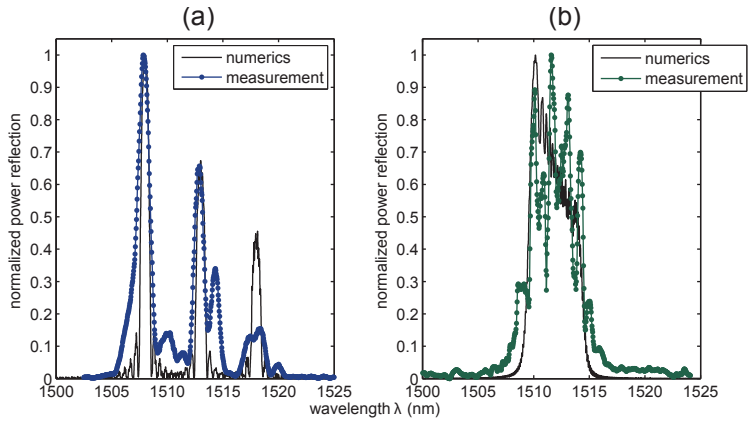

Figure 5. Experimental reflection spectra of a multi–period (a) and a chirped WBG (b). The corresponding numerical calculation is shown by the black solid line. The total length of the waveguide is 10 mm in both cases. Three 1 mm long gratings with a period of 706.1 nm, 708.4 nm and 710.7 nm are inscribed in case of the multi–period structure and the individual reflection maxima can be clearly seen. The chirped WBG consists of a 5 mm long grating that is linearly chirped from 706.1 nm to 708.4 nm. The associated increase of the reflection bandwidth is clearly visible although the coupling strength is limited.

relative shift of the central Bragg reflection maxima versus drive voltage are shown in Fig. 4(b) and Fig. 4(c). It can be seen that the spectra shifts by approximately a peak half width ($\lambda'_e = \pm 594\,\mathrm{pm}$) without any spectral deformations indicating a uniform field distribution and pure single–mode transmission.

The central Bragg wavelength $\lambda_{o,e}$ is shifted according to the linear Pockels effect. For second–order gratings, the Bragg equation simplifies to $\lambda'_{o,e} = (n_{o,e} + \Delta n_{NL})\Lambda$ where $\Delta n_{NL} = -0.5 n^3_{o,e} r_{13,33} U/d$ denotes the induced nonlinear refractive index change. The electro–optic coefficients for light polarized along the principle crystallographic axis are referred to as $r_{13,33}$ and U denotes the applied voltage over a distance d. Figure 4(c) depicts the relative shift $\Delta\lambda = \lambda' - \lambda_{o,e}$ of the central Bragg reflection wavelength as a function of the applied voltage for ordinary and extraordinary input polarizations. Both traces exhibit perfectly linear characteristics, therefore the electro–optical coefficients can be precisely determined by linear regression. Nearly preserved electro–optic coefficients of $r_{13} = 7.67\,\mathrm{pm\,V^{-1}}$ (s–pol) and $r_{33} = 24.7\,\mathrm{pm\,V^{-1}}$ (p–pol) are obtained, which corresponds to more than 80 % of bulk lithium niobate.[19] Similar coefficients are measured for the entire series of WBGs indicating that the small reduction of the nonlinear response is a property of the waveguide rather than it is induced by the modification of the core region. Furthermore, frequency tests are performed with a modulation frequency up to 2 MHz without any degradation of the nonlinear response.

5. CHIRPED AND MULTI–PERIOD GRATINGS

As previously described, the unique feature of the direct laser writing approach is the possibility to fabricate arbitrary modulation patterns without any demand for special lithographic masks. To demonstrate this feature and to outline prospects for integrated optical devices and next generation optical networks, we fabricated a multi–period WBG as well as a linearly chirped WBG. The spectral response and the corresponding numerical calculation (including the propagation loss) is shown Fig. 5(a) and Fig. 5(b).

The multi–period WBG (c. f. Fig. 5(a)) consists of a 10 mm long circular waveguide with three 1 mm long embedded Bragg gratings that are inscribed with a pulse energy of 3.65 nJ. The design wavelength of the individual gratings are $\lambda_1 = 1508\,\mathrm{nm}$, $\lambda_2 = 1513\,\mathrm{nm}$ and $\lambda_3 = 1518\,\mathrm{nm}$. All three reflection maxima are clearly observed, which also demonstrates that the gratings exhibit a sufficiently high transmission. A propagation loss of $\alpha_e = -8.51\,\mathrm{dB\,cm^{-1}}$ and a refractive index modulation of $\Delta n_e = 8 \times 10^{-4}$ is obtained for the multi–period grating. In principle a longer device could be fabricated with a series of narrow–spaced reflection channels. Every single Bragg grating could be separately addressed by integrated micro electrodes enabling compact, on–chip wavelength filtering.

Figure 5(b) shows the spectral response of a linearly chirped WBG. The 5 mm long grating is inscribed with a pulse energy of 3.45 nJ. The design period is linearly chirped from $\Lambda_1 = 706.1\,\mathrm{nm}$ to $\Lambda_2 = 708.4\,\mathrm{nm}$ which corresponds to a design reflection bandwidth of $\lambda_1 = 1508\,\mathrm{nm}$ to $\lambda_2 = 1513\,\mathrm{nm}$. The strong broadening of the reflection maxima to approximately $\Delta\lambda = 5\,\mathrm{nm}$ can be clearly seen. In accordance to the previous case of multi–period gratings and the performed numerical calculation, the available coupling strength is relatively weak. We obtained an approximated refractive index modulation of $\Delta n_e = 4.3 \times 10^{-4}$, which also explains the weak power reflection. However, the principle of chirped WBGs is successfully demonstrated and the presented approach could be applied to much longer gratings. It should be mentioned that the available coupling strength was not optimized in case of the multi–period, and chirped gratings. Thus it can be expected that slightly higher pulse energies around 3.8 nJ as shown in the previous section will directly lead to a significantly improved spectral response.

6. CONCLUSION

In conclusion, second–order multiscan Bragg gratings are embedded into the core volume of a circular two–dimensional waveguide in $LiNbO_3$. In addition to uniform Bragg gratings, multi–period and chirped gratings are realized that potentially allow tunable multi–channel filtering devices and on–chip dispersion compensation. The hybrid type-I/II structure exhibits low loss, symmetric guiding with superior mode fidelity and narrowband reflection in the c–band of optical communications. Nearly preserved electro–optic coefficients of $r_{13} = 7.67\,\mathrm{pm\,V^{-1}}$ (s–pol) and $r_{33} = 24.7\,\mathrm{pm\,V^{-1}}$ (p–pol) facilitate spectral tuning of more than a peak half width, which is a key feature for functional optical devices and high bandwidth signal processing. Such complex waveguide embedded structures are the key step towards all-integrated circuits for nonlinear signal processing and filtering applications by direct femtosecond laser writing.

ACKNOWLEDGMENTS

We especially thank TOPAG for providing the femtosecond laser system for this project.

REFERENCES

[1] Gattass, R. R. and Mazur, E., "Femtosecond laser micromachining in transparent materials," *Nat Photon* **2**, 219–225 (2008).

[2] Della Valle, G., Osellame, R., and Laporta, P., "Micromachining of photonic devices by femtosecond laser pulses," *Journal of Optics A: Pure and Applied Optics* **11**, 013001 (2009).

[3] Osellame, R., Cerullo, G., and Ramponi, R., [*Femtosecond Laser Micromachining: Photonic and Microfluidic Devices in Transparent Materials*], Springer (2012).

[4] Thomas, J., Heinrich, M., Zeil, P., Hilbert, V., Rademaker, K., Riedel, R., Ringleb, S., Dubs, C., Ruske, J., Nolte, S., and Tünnermann, A., "Laser direct writing: Enabling monolithic and hybrid integrated solutions on the lithium niobate platform," *physica status solidi (a)* **208**, 276–283 (2011).

[5] Chen, F. and de Aldana, J. R. V., "Optical waveguides in crystalline dielectric materials produced by femtosecond-laser micromachining," *Laser & Photonics Reviews* **8**(2), 251–275 (2014).

[6] Kroesen, S., Horn, W., Imbrock, J., and Denz, C., "Electrooptical tunable waveguide embedded multiscan Bragg gratings in lithium niobate by direct femtosecond laser writing," *Optics Express* **22**, 23339–23348 (2014).

[7] Rdenas, A., Nejadmalayeri, A. H., Jaque, D., and Herman, P., "Confocal raman imaging of optical waveguides in $LiNbO_3$ fabricated by ultrafast high-repetition rate laser-writing," *Optics Express* **16**, 13979–13989 (2008).

[8] Rodenas, A., Maestro, L. M., Ramirez, M., Torchia, G. A., Roso, L., Chen, F., and Jaque, D., "Anisotropic lattice changes in femtosecond laser inscribed Nd^{3+}:MgO:$LiNbO_3$ optical waveguides," *Journal of Applied Physics* **106**, 013110–013110–6 (2009).

[9] Thomson, R. R., Campbell, S., Blewett, I. J., Kar, A. K., and Reid, D. T., "Optical waveguide fabrication in z-cut lithium niobate ($LiNbO_3$) using femtosecond pulses in the low repetition rate regime," *Applied Physics Letters* **88**, 111109–111109–3 (2006).

[10] Burghoff, J., Hartung, H., Nolte, S., and Tünnermann, A., "Structural properties of femtosecond laser-induced modifications in $LiNbO_3$," *Applied Physics A* **86**, 165–170 (2006).

[11] Burghoff, J., Nolte, S., and Tünnermann, A., "Origins of waveguiding in femtosecond laser-structured $LiNbO_3$," *Applied Physics A* **89**, 127–132 (2007).

[12] Horn, W., Kroesen, S., Herrmann, J., Imbrock, J., and Denz, C., "Electro-optical tunable waveguide Bragg gratings in lithium niobate induced by femtosecond laser writing," *Optics Express* **20**, 26922–26928 (2012).

[13] Okhrimchuk, A. G., Shestakov, A. V., Khrushchev, I., and Mitchell, J., "Depressed cladding, buried waveguide laser formed in a YAG:Nd^{3+} crystal by femtosecond laser writing," *Optics Letters* **30**, 2248–2250 (2005).

[14] Salamu, G., Jipa, F., Zamfirescu, M., and Pavel, N., "Laser emission from diode-pumped Nd:YAG ceramic waveguide lasers realized by direct femtosecond-laser writing technique," *Optics Express* **22**(5), 5177–5182 (2014).

[15] Salamu, G., Jipa, F., Zamfirescu, M., and Pavel, N., "Cladding waveguides realized in Nd:YAG ceramic by direct femtosecond-laser writing with a helical movement technique," *Optical Materials Express* **4**, 790–797 (2014).

[16] Gross, S., Ams, M., Lancaster, D. G., Monro, T. M., Fuerbach, A., and Withford, M. J., "Femtosecond direct-write berstructure waveguide Bragg gratings in ZBLAN," *Optics Letters* **37**(19), 3999–4001 (2012).

[17] Liao, Y., Xu, J., Cheng, Y., Zhou, Z., He, F., Sun, H., Song, J., Wang, X., Xu, Z., Sugioka, K., and Midorikawa, K., "Electro-optic integration of embedded electrodes and waveguides in $LiNbO_3$ using a femtosecond laser," *Optics Letters* **33**(19), 2281–2283 (2008).

[18] Pozza, G., Kroesen, S., Bettella, G., Zaltron, A., Esseling, M., Mistura, G., Sartori, P., Chiarello, E., Pierno, M., Denz, C., and Sada, C., "T-junction droplet generator realised in lithium niobate crystals by laser ablation," *Optofluidics, Microfluidics and Nanofluidics* **1** (2014).

[19] Lee, S. H., Kim, S. H., Kim, K. H., Lee, M. H., and Lee, E.-H., "A novel method for measuring continuous dispersion spectrum of electro-optic coefficients of nonlinear materials," *Optics Express* **17**, 9828–9833 (2009).